subdomain VI of the catalytic portion with a neomycin resistance gene. The neomycin resistance gene was flanked by the 5.6-kb 5′ genomic fragment and the 1.1-kb 3′ fragment. A herpes simplex virus–thymidine kinase cassette was introduced at the 5′ end of the genomic fragment. E14.1 ES cells were transfected with the linearized targeting vector and selected by addition of G418 and gancyclovir. Two independently targeted ES clones were microinjected into C57BL/6 blastocysts, and the resulting chimeric mice from both clones successfully transmitted the targeted allele through the germ line. Generation of the homozygotes was done essentially as described [K. Takeda *et al*., *Nature* **380**, 627 (1996)].
6. P. B. Bushdid *et al*., *Nature* **392**, 615 (1998); Y. Kanegae *et al*., *ibid*. p. 611.
7. The desired fragments of mouse *IKKα*, *IKKβ*, *BMP4*, and *Twist* cDNAs were subcloned into pBluescript (Stratagene). Complementary RNA probes were then prepared by using a digoxigenin RNA labeling kit (Boehringer Mannheim). Embryos at 12.5 dpc were fixed in 4% paraformaldehyde in phosphate-buffered saline (PBS) for 5 hours at 4°C with rocking. Embryos were washed with PBS containing 0.1% Tween 20, treated with a mixture of methanol and 30% hydrogen peroxide (5:1 in volume) for 5 hours at room temperature, dehydrated into 100% methanol, and stored at −20°C. For hybridization, embryos were incubated at 65°C overnight in hybridization buffer with digoxigenin-labeled complementary RNA probes (0.4 μg/ml). Hybridized digoxigenin-labeled probes were detected with a nucleic acid detection kit (Boehringer Mannheim).
8. J. Jiang, D. Kosman, Y. T. Ip, M. Levine, *Genes Dev*. **5**, 1881 (1991); D. Pan, J.-D. Huang, A. J. Courey, *ibid*., p. 1892; J. D. Huang, D. H. Schwyer, J. M. Shirokawa, A. J. Courey, *ibid*. **7**, 694 (1993); D. H. Schwyer, J. D. Huang, T. Dubnicoff, A. J. Courey, *Mol. Cell. Biol*. **15**, 3960 (1995).
9. I. Gitelman, *Dev. Biol*. **189**, 205 (1997).
10. V. E. Ghouzzi, *Nature Genet*. **15**, 42 (1997); T. D. Howard *et al*., *ibid*., p. 41.
11. K. Takeda and T. Tsujimura, unpublished data.
12. M. Saitou *et al*., *Nature* **374**, 159 (1995); M. Matsuki *et al*., *Proc. Natl. Acad. Sci. U.S.A*. **95**, 1044 (1998).
13. C. S. Seitz, Q. Lin, H. Deng, P. A. Khavari, *Proc. Natl. Acad. Sci. U.S.A*. **95**, 2307 (1998).
14. S. Ma, L. Rao, I. M. Freedberg, M. Blumenberg, *Gene Exp*. **6**, 361 (1997); M. Tomic-Canic, M. Komine, I. M. Freedberg, M. Blumenberg, *J. Dermatol. Sci*. **17**, 167 (1998).
15. Pieces of the dorsal skin were removed, fixed in 10% buffered formalin, and used for paraffin sections. The deparaffin was removed and sections were incubated with anti-IκBα, anti-IκBβ, or anti-RelA (Santa Cruz) at 4°C overnight. After they were washed, the sections were incubated with biotin-conjugated goat antibody to rabbit immunoglobulin G (Dako A/S) for 60 min, which was visualized with streptavidin-peroxidase (Vecstatin ABC Elite kit; Vector Laboratories) and diaminobenzene (Sigma). Some of the sections were lightly counterstained with hematoxylin.
16. EF cells were stimulated with TNF-α (50 ng/ml) or IL-1β (1000 U/ml) and lysed. Proteins from cell lysates were separated on SDS-polyacrylamide gels, transferred to nitrocellulose membranes, and incubated with antibodies to IκBα, IκBβ, IKKα, or IKKβ (Santa Cruz). Bound antibody was visualized with an enhanced chemiluminescence system (DuPont). Preparation of nuclear extracts and electrophoretic mobility shift assays were done as described [O. Adachi *et al*., *Immunity* **9**, 143 (1998)].
17. S. Ghosh, M. J. May, E. B. Kopp, *Annu. Rev. Immunol*. **16**, 225 (1998).
18. A. A. Beg, W. C. Sha, R. T. Bronson, S. Ghosh, D. Baltimore, *Nature* **376**, 167 (1995).
19. Pieces of the dorsal skin were removed and used for frozen sections. After fixation with cold acetone, frozen sections (5 μm) were incubated with primary antibodies for 1 hour at room temperature, washed in PBS, and incubated with fluorescein isothiocyanate–conjugated second antibodies. Slides were then analyzed by fluorescence microscopy. Primary antibodies used in this study were as follows: mouse antibody to K14 (LL002, Novocastra), rabbit antibody to keratin 10 (BAbCO), rabbit antibody to involucrin (BAbCO), mouse antibody to filaggrin (Biomedical Technologies), and rabbit antibody to Ki67 (Novocastra).
20. We thank A. Kuhara for technical assistance, T. Aoki for secretarial assistance, and M. Suda and K. Tanaka for technical comments. Supported by grants from the Ministry of Education of Japan.

15 December 1998; accepted 12 March 1999

Abnormal Morphogenesis But Intact IKK Activation in Mice Lacking the IKKα Subunit of IκB Kinase

Yinling Hu,[1] Véronique Baud,[1]* Mireille Delhase,[1]* Peilin Zhang,[2] Thomas Deerinck,[3] Mark Ellisman,[3] Randall Johnson,[4] Michael Karin[1]†

The oligomeric IκB kinase (IKK) is composed of three polypeptides: IKKα and IKKβ, the catalytic subunits, and IKKγ, a regulatory subunit. IKKα and IKKβ are similar in structure and thought to have similar function—phosphorylation of the IκB inhibitors in response to proinflammatory stimuli. Such phosphorylation leads to degradation of IκB and activation of nuclear factor κB transcription factors. The physiological function of these protein kinases was explored by analysis of IKKα-deficient mice. IKKα was not required for activation of IKK and degradation of IκB by proinflammatory stimuli. Instead, loss of IKKα interfered with multiple morphogenetic events, including limb and skeletal patterning and proliferation and differentiation of epidermal keratinocytes.

NF-κB/Rel proteins are dimeric transcription factors whose activity is regulated by interaction with IκB inhibitors (*1*). In nonstimulated cells NF-κB proteins are retained in the cytoplasm because IκBs mask their nuclear localization sequence. Exposure to proinflammatory stimuli results in rapid phosphorylation, ubiquitilation, and degradation of the IκBs (*1*). Freed

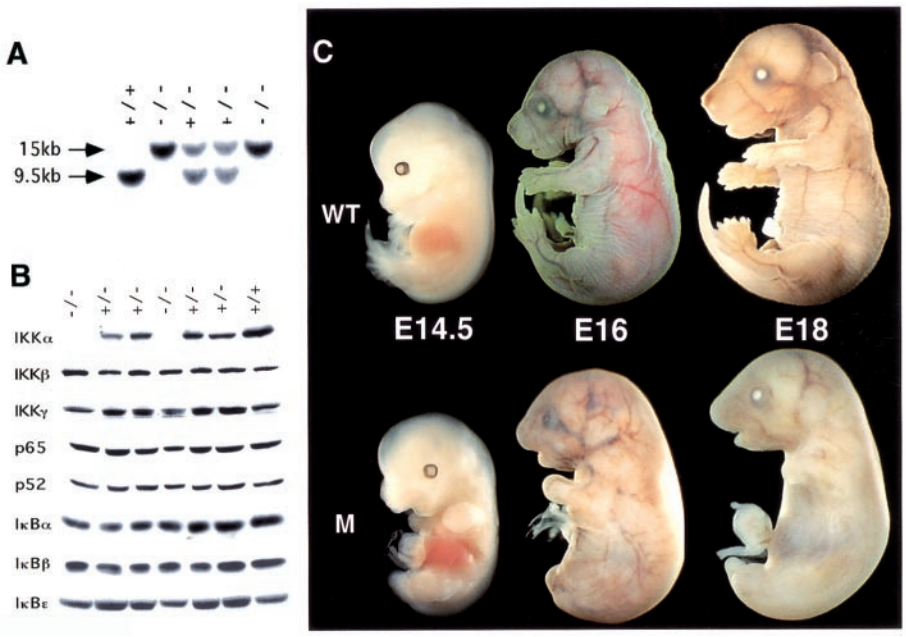

Fig. 1. Phenotypic and genotypic analysis of IKKα-deficient mice. (**A**) Southern blot analysis of Sac I–digested genomic DNA derived from E18 fetuses of different genotypes. (**B**) Protein immunoblot analysis of protein extracts prepared from muscle tissue of E18 fetuses of the indicated genotypes. Extracts were separated by SDS-PAGE, transferred to a nylon membrane, and probed with antibodies against the indicated proteins. (**C**) Appearance of wild-type (WT) and *Ikkα*$^{-/-}$ (M) fetuses collected at E14.5, E16, and E18. The tight and smooth appearance of mutant skin is apparent.

NF-κB dimers translocate to the nucleus and regulate target gene transcription. The protein kinase that phosphorylates IκBs in response to proinflammatory stimuli is a multiprotein complex, the IκB kinase (IKK), composed of two catalytic subunits, IKKα and IKKβ (*2*–*4*), and a regulatory subunit, IKKγ or NEMO (*5*, *6*). In several human cell lines the IKK complex consists of stable IKKα:IKKβ heterodimers tightly associated with dimers or trimers of IKKγ (*5*). In vitro, IKKα and IKKβ can form homo- and heterodimers that directly phosphorylate IκBs at their regulatory serines (*4*). IKKβ, but not IKKα, associates directly with IKKγ, which links the IKK complex to upstream activators (*5*). Apart from this, IKKα and IKKβ were both believed to be functionally similar and required for IKK and NF-κB activation (*2-4*). However, we recently found that IKKβ, and not IKKα, serves as the target for proinflammatory stimuli that lead to IKK activation (*7*).

To determine the biological functions of IKKα, we generated mice deficient in that subunit. These mice exhibited normal activation of IKK and degradation of IκB in response to proinflammatory stimuli but displayed multiple morphogenetic defects.

Mouse *Ikk*α genomic DNA was used to construct the targeting vector (*8*). To eliminate kinase activity, a part of the exon that encodes the adenosine 5′-triphosphate binding site (amino acids 192 to 212) was replaced with a DNA fragment encoding β-galactosidase (*LacZ*) and neomycin resistance (*Neo*^{r}) (*8*). Because the *Neo*^{r} gene contains transcription termination and polyadenylation signals, the COOH-terminal two-thirds of IKKα, which contains its leucine zipper and helix-loop-helix protein interaction motifs (*2*), was not expressed in mutant cells (*9*).

Using this vector and positive-negative selection (*10*), we isolated three embryonic stem (ES) cell clones with a disrupted *Ikk*α allele. Chimeric mice derived from these cells transmitted the disrupted allele to their progeny (*11*). *Ikk*α$^{+/-}$ mice were viable, healthy, and fertile and had normal appearance. Intercrossed

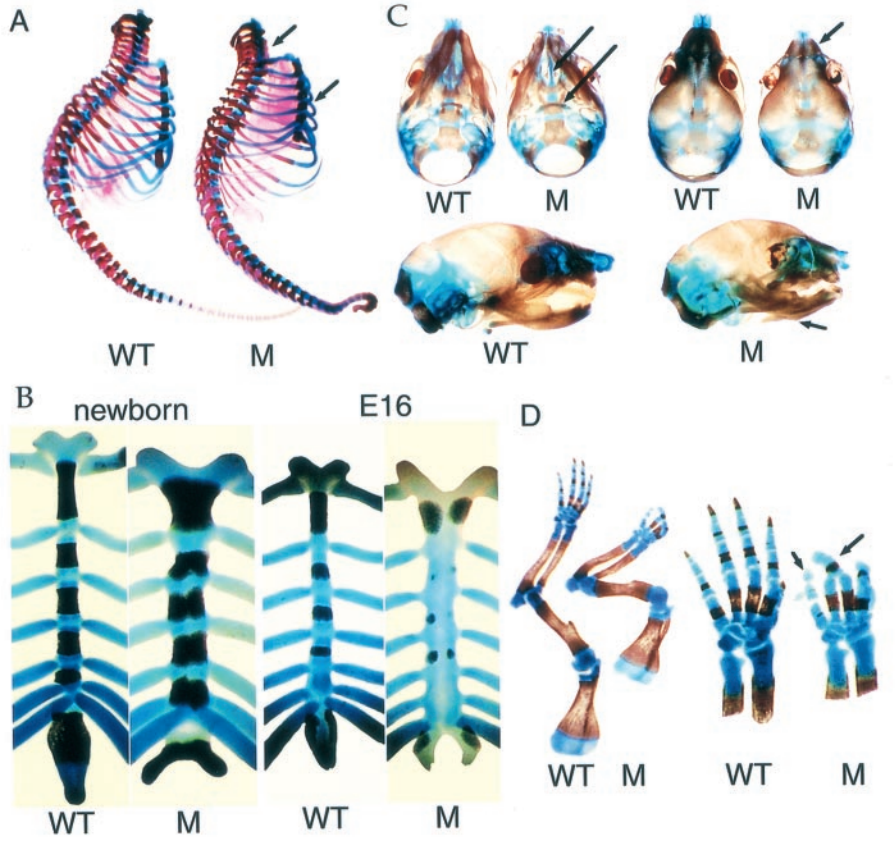

Fig. 2. Skeletal structures of wild-type (WT) and mutant (M) mice. (**A**) Vertebral columns and rib cages of newborn mice stained with alcian blue and alizarin red. (**B**) Sterna of newborn and E16 mice stained as above. (**C**) Skulls of E18 fetuses were stained as above and photographed from the bottom (top left), top (top right), and side (bottom). (**D**) Forelimb bones of E18 fetuses. Some of the more obvious skeletal defects are indicated by arrows. Similar results were obtained with five skeletal preparations.

[1]Laboratory of Gene Regulation and Signal Transduction, Department of Pharmacology, and [2]Departments of Pathology, [3]Neuroscience, and [4]Biology, Cancer Center, University of California San Diego, La Jolla, CA 92093–0636, USA.

*These authors contributed equally to this work.
†To whom correspondence should be addressed. E-mail: karinoffice@ucsd.edu

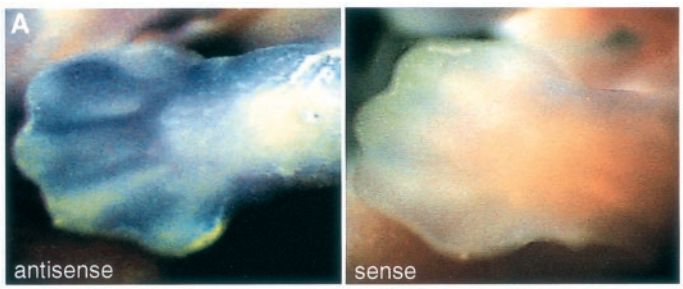

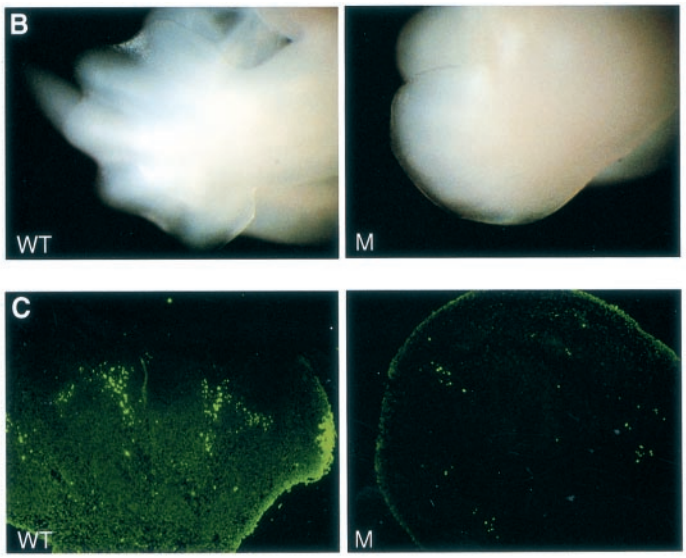

Fig. 3. Analysis of paw development in wild-type (WT) and mutant (M) embryos. (**A**) In situ whole-mount hybridization with antisense and sense *Ikk*α probes of forepaws from E13 embryos. (**B**) Photomicrographs of forepaws from E13 WT and mutant embryos. (**C**) TUNEL staining of sectioned forepaws from E13 embryos.

Ikkα$^{+/-}$ females bore normal numbers of embryos (5 to 11), of which ~24% (32 out of 133) had abnormal appearance. Genotyping revealed that all abnormal embryos were homozygous for the disrupted allele (Fig. 1A). Analysis of extracts (*12*) prepared from fetuses collected at embryonic day 18 (E18) revealed no expression of IKKα in *Ikkα*$^{-/-}$ fetuses and decreased expression in heterozygotes (Fig. 1B). No changes in expression of IKKβ, IKKγ, the p65 and p52 subunits of NF-κB, IκBα, IκBβ, or IκBε were detected. Similar results were obtained by RNA analysis (*9*).

At E18, *Ikkα*$^{-/-}$ mutant fetuses had rudimentary protrusions instead of normal limbs (Fig. 1C). In addition, they lacked well-formed tails, and their heads were shorter than normal, with a truncated snout and no external ears. E18 mutant fetuses also had an omphalocele (a gastrointestinal protrusion into the umbilical cord). In E16 mutant embryos, forelimbs (but not hindlimbs) were visible but were considerably shorter than those of normal (*Ikkα*$^{+/+}$ and *Ikkα*$^{+/-}$) littermates and lacked separated digits. In addition, E16 and E18 *Ikkα*$^{-/-}$ fetuses had taut skin, lacking folds or wrinkles visible on normal counterparts. At an earlier stage, E14.5, the fore- and hindlimbs of mutant embryos were not much shorter than those of normal counterparts, but were devoid of distinct digits.

Ikkα$^{-/-}$ embryos developed to term and were born alive, but died within 30 min. The *Ikkα*$^{-/-}$ neonates were smaller than normal and had the same appearance as the mutant E18 fetuses (*9*). Autopsy revealed no obvious morphological abnormalities of the heart, lungs, liver, kidneys, spleen, brain, and spinal cord (*13*). Mutant placentae, however, were severely congested with bulging vessels and blood sinuses on the maternal surface and normal fetal surface (*13*). These findings suggest that the cause of death is cardiovascular malfunction (*14*). The cardiac muscle itself was morphologically normal (*13*). Consistent with the pleiotropic developmental defects caused by the loss of IKKα, in situ hybridization revealed widespread expression of the gene, highest in the developing spine, limb buds, and head (*9*).

Examination of skeletal preparations stained with alcian blue (to reveal cartilage) and alizarin red (an indicator of calcification) revealed multiple abnormalities (Fig. 2). Although *Ikkα*$^{-/-}$ embryos had normal numbers of lumbar and thoracic vertebrae, many of the sacral vertebrae were small and fused (Fig. 2A). Cervical vertebrae were fused as well. As a result of a shorter sternum the mutants had smaller thoracic cages. Mutant sterna failed to fuse and exhibited delayed ossification (Fig. 2B). The xiphoid process also failed to fuse and was bifurcated. Skulls of mutant fetuses were smaller (mostly shorter) and maldeveloped (Fig. 2C). Some of the skull bones were missing or reduced in size. Strikingly, despite the almost complete absence of external limbs, the mutants had modestly truncated limb bones with close to normal shape under their skin (Fig. 2D). The bones were surrounded by normal-appearing muscle. Closer examination revealed syndactyly in both fore- and hindpaws of *Ikkα*$^{-/-}$ embryos (Fig. 2D) (*9*). Mutant digits were half as long as normal and partially mineralized. The first phalanges of digits III and IV were fused, whereas the second and third phalanges were absent. Mutant hindpaws had similar features to the forepaws except for complete absence of phalanges (*9*).

During paw development mesodermal cells in the limb bud condense to give rise to the cartilage matrix for elements of the five digits,

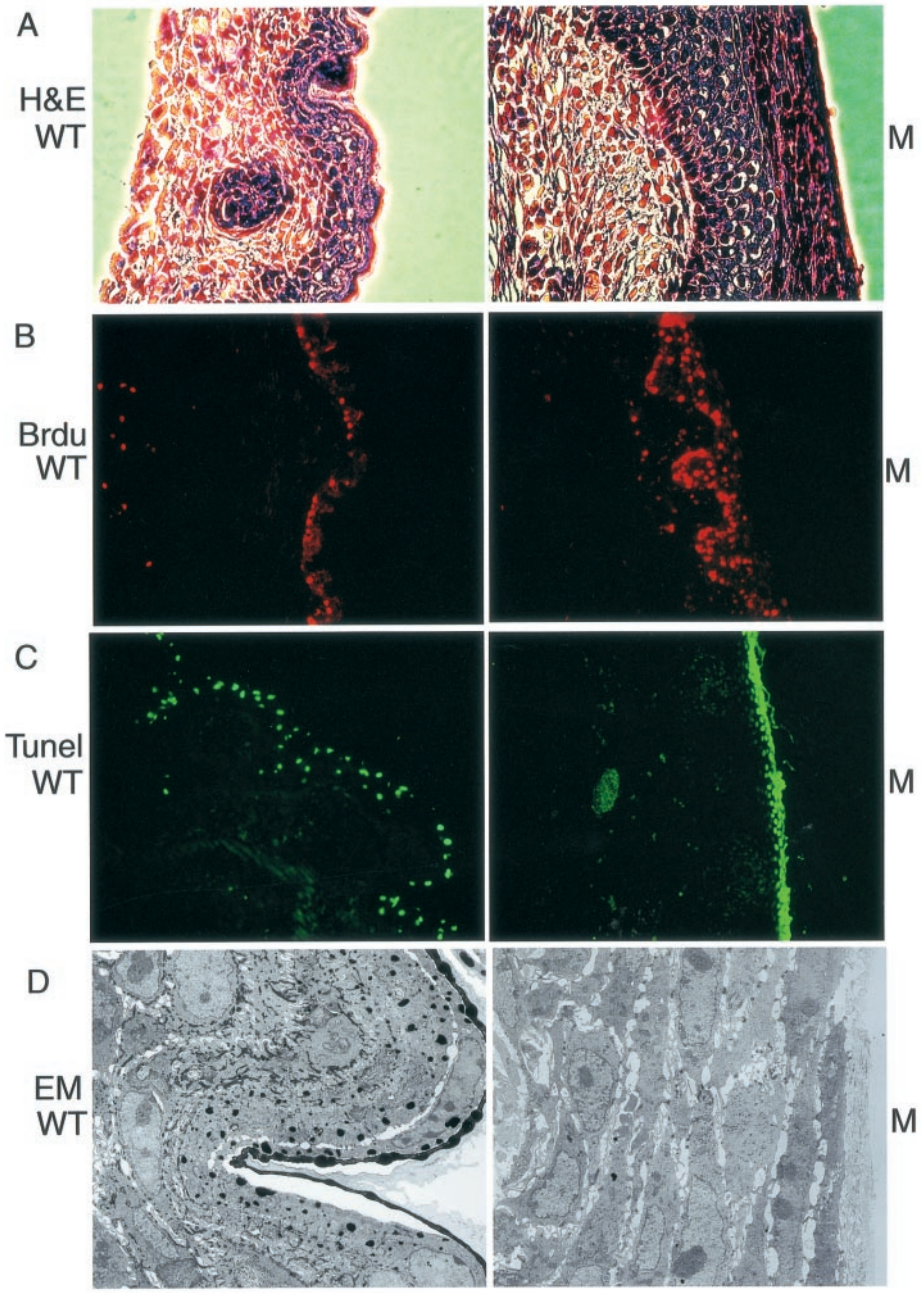

Fig. 4. Analysis of wild-type (WT) and mutant (M) skin. (**A**) Sections of back skin of E17 fetuses were stained with hematoxylin and eosin (H&E). (**B**) E17 mouse embryos were isolated 2 hours after their mothers were injected with BrdU and fixed in 4% paraformaldehyde. Paraffin sections were stained with anti-BrdU and visualized by fluorescence immunohistochemistry. (**C**) Paraffin sections of back skin from E19 fetuses were analyzed by TUNEL staining. Magnification: (A) to (C), ×285. (**D**) Electron micrographs of normal and mutant epidermis. Pieces of skin from the mid-thoracic region of fixed E17 fetuses were examined by electron microscopy (magnification: WT, ×2100; mutant, ×2010) after sectioning and staining with lead citrate. In all images the outer edge of the epidermis points to the right. The complete absence of the two outer layers in mutant epidermis is apparent.

the carpals and the long bones (*15*). In most mammals, cells in the interdigital region undergo programmed cell death, thus creating distinct digits. In situ hybridization revealed abundant expression of *Ikk*α mRNA in both the digital and interdigital region of the E13 autopod (Fig. 3A). At E13, the mutant paws failed to form distinct digits, resulting in webbed morphology (Fig. 3B). TUNEL (terminal deoxynucleotidyl transferase–mediated dUTP nick-end labeling) staining (*16*) revealed a reduced number of apoptotic cells in the interdigital areas of the mutant E13 paw (Fig. 3C).

Mutant embryos lacked obvious ridges or wrinkles on their skin (Fig. 1C). Microscopic examination of back skin sections from wild-type (WT) and mutant E18 fetuses confirmed this and revealed hyperplasia of the suprabasal layer (stratum spinosum) of mutant epidermis (Fig. 4A). This may explain the tightness of the mutant skin. In vivo labeling (*17*) with bromodeoxyuridine (BrdU) indicated that the increased thickness of the suprabasal layer was due to a higher rate of cell proliferation (Fig. 4B). Although TUNEL staining revealed large number of apoptotic cells at the outer edge of mutant epidermis (Fig. 4C), this may be due to the larger number of epidermal progenitors that arrive at this zone where terminal differentiation and cell death through surface desquamation give rise to the cornified layer (which is absent in the mutant). In normal epidermis most programmed cell death occurred within the stratum spinosum. Electron microscopy revealed that in addition to marked increase in the thickness of the stratum spinosum, mutant epidermis was completely missing the two upper layers, the stratum granulosum and stratum corneum (Fig. 4D). Therefore, the loss of IKKα results in a complete block of keratinocyte differentiation.

Transverse sections at the hindlimb level revealed that whereas normal limbs and tail were well separated from the body, the mutant limbs and tail were surrounded by a thick layer of skin that was fused to the skin cover of the body (Fig. 5A). This suggests increased self-adhesion of mutant epidermis in supplementary Web Fig. 2 (*18*). A similar defect may be responsible for closure of the esophagus in *IKK*$\alpha^{-/-}$ fetuses (Fig. 5B). The inside of this organ is also covered with keratinocytes.

To determine whether loss of IKKα affects the regulation of IκB phosphorylation and degradation, we cultured fibroblasts from *Ikk*$\alpha^{+/+}$ and *Ikk*$\alpha^{-/-}$ E13 embryos. Treatment of *Ikk*$\alpha^{-/-}$ cells with tumor necrosis factor (TNF) or interleukin-1 (IL-1) resulted in normal stimulation of IκB kinase activity measured by immune complex kinase assays with antibodies to either IKKβ or IKKγ, although no IKKα-associated kinase activity was detected (Fig. 6A). We also detected normal induction of IKBα degradation and resynthesis (Fig. 6B) and nuclear translocation of p65/RelA (Fig. 6C) in *Ikk*$\alpha^{-/-}$ cells. Mobility shift assays indicated that TNF treatment of *Ikk*$\alpha^{-/-}$ fibroblasts resulted in induction of NF-κB DNA binding activity (*19*). Because the function of IKKα may be cell type–specific, we also examined the regulation of IKK activity in WT and mutant livers. E18 fetuses were exposed by Cesarean sec-

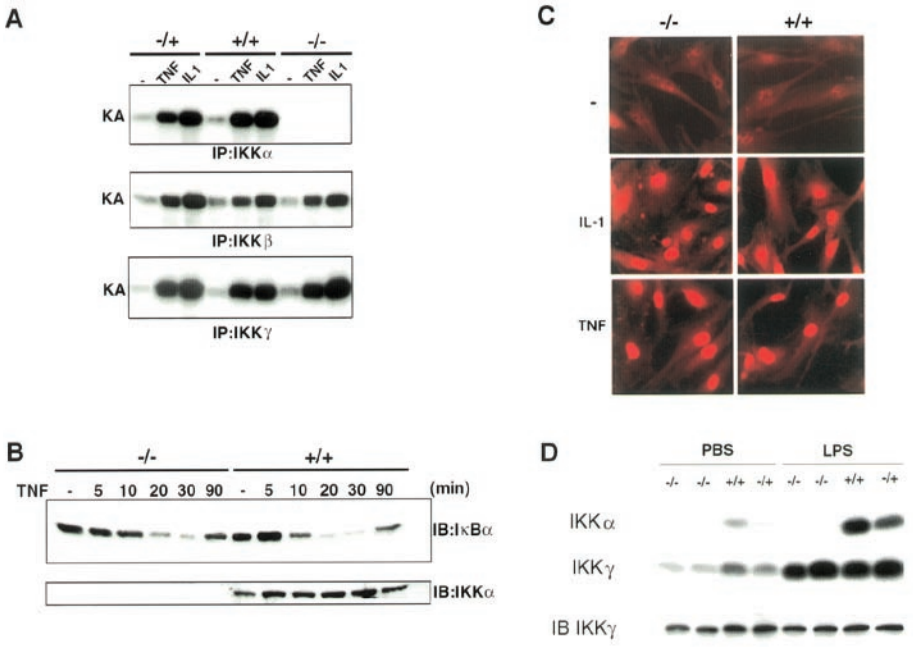

Fig. 6. IKK and NF-κB activation in the absence of IKKα. (**A**) IKK activation in fibroblasts. Primary cultures of mouse embryonic fibroblasts (MEFs) from E13 embryos were left untreated or stimulated for 10 min with mouse TNF (10 ng/ml) or IL-1 (10 ng/ml). IKK complexes were isolated from cell lysates by immunoprecipitation (IP) with anti-IKKα, anti-IKKβ, or anti-IKKγ, and associated kinase activity was determined with glutathione S-transferase–IκBα(1–54) as a substrate (*2*). (**B**) IκBα degradation. MEFs were incubated with TNF for the indicated times, then lysed. IκBα degradation was monitored by immunoblotting with anti-IκBα (Santa Cruz). The same blot was reprobed with anti-IKKα. (**C**) Cytokine-induced nuclear translocation of RelA(p65). MEFs grown on Lab-Tek chamber slides were left untreated or stimulated for 30 min with mouse TNF or IL-1. Cells were fixed and the subcellular distribution of RelA was examined by fluorescent immunostaining with anti-RelA(p65). (**D**) Activation of IKK in fetal liver. Wild-type and mutant E17 fetuses were exposed by a cesarean section and injected intraperitoneally with 5 μg of LPS in PBS or with PBS alone. After 40 min the fetuses were removed and protein extracts were prepared from their livers. IKK complexes were isolated by immunoprecipitation with either anti-IKKα or anti-IKKγ and their kinase activity determined as described above. The amount of IKKγ was determined by immunoblotting.

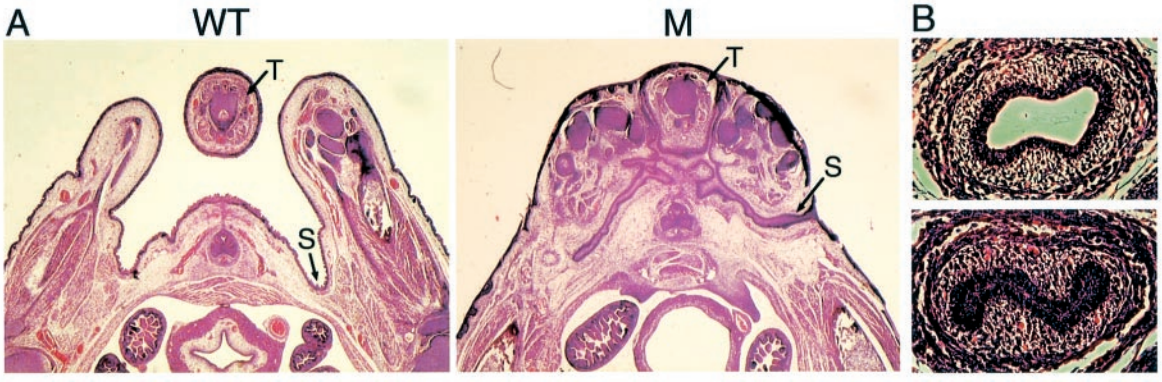

Fig. 5. Defects caused by increased adhesiveness of mutant epidermis. (**A**) Transverse sections of wild-type (WT) and mutant (M) E17 fetuses at the hindlimb level stained with H&E. S, skin; T, tail. (**B**) Section of wild-type (top) and mutant (bottom) esophagus from E17 fetuses stained with H&E.

tion of anesthetized mothers and while in utero were injected with lipopolysaccharide (LPS), a potent NF-κB activator. This resulted in efficient IKK activation, measured by immune complex kinase assays with anti-IKKγ in both WT and mutant livers (Fig. 6D). Immunohistochemical analysis revealed normal LPS-induced nuclear translocation of p65/RelA in mutant livers (*20*).

These results indicate that mice and cells that lack IKKα exhibit normal activation of the variant IKK complex they express [presumably composed of IKKβ homodimers and IKKγ and still eluting from a sizing column at 900 kD (*19*)] in response to proinflammatory stimuli, resulting in IκB phosphorylation and degradation. This is not the result of functional redundancy between IKKα and IKKβ because mice and cells that lack IKKβ exhibit the expected defects in IKK and NF-κB activation (*21*). In addition, biochemical and reverse genetic analysis indicate that IKKβ, and not IKKα, is the target for upstream signals generated by proinflammatory stimuli (*7*). Instead of responding to proinflammatory signals, IKKα appears to participate in multiple morphogenetic processes, including limb development, apoptosis of interdigital tissue, and proliferation and differentiation of epidermal keratinocytes. None of these functions appears to be compensated by IKKβ. However, it is not clear whether the developmental and morphogenetic function of IKKα is executed by standard IKK complexes, composed of IKKα: IKKβ heterodimers and IKKγ (*5*), or by IKKα homodimers that may be associated with another regulatory subunit.

In *Drosophila melanogaster* NF-κB transcription factors participate in both pattern formation and innate immunity (*22*). Knockout mice deficient in individual NF-κB proteins provide genetic evidence for their function in various aspects of innate and acquired immunity but not in development or morphogenesis (*23*). Given the high degree of functional conservation between insect and mammalian dorsal/NF-κB pathways, the absence of developmental function for mammalian NF-κB proteins is puzzling. Yet, expression of a phosphorylation-defective IκBα mutant in the chicken limb bud interfered with development (*24*). These results, however, could be caused by elimination of the anti-apoptotic function of NF-κB (*25*), resulting in ablation of cells in the progress zone of the limb bud. In fact, the defects in limb development caused by loss of IKKα are much milder and different from those caused by overexpression of mutant IκBα. Expression of the IκBα mutant in mouse skin produced a phenotype that is superficially similar to the one caused by loss of IKKα, namely, hyperplasia of the suprabasal layer (*26*). Yet, expression of the IκBα mutant did not block epidermal differentiation, suggesting that the effect of the IKKα mutation is not simply due to a defect in NF-κB activation.

The most striking defect associated with loss of IKKα expression is the failure to form stratified, well-differentiated epidermis. It appears that the increased thickness and adhesiveness of the mutant skin causes it to act as a capsule that prevents the emergence of limb outgrowths. In addition, the defect in epidermal differentiation may perturb production of morphogens by epidermal thickenings, such as the apical ectodermal ridge (AER). This may account, in part, for the defects in skeletal patterning observed in *Ikkα*$^{-/-}$mice, some of which resemble defects in mice that are deficient in certain bone morphogenetic proteins (BMPs). For example, a partially split sternum and forked xiphoid with delayed ossification were observed in BMP5 and BMP6 doubly deficient mice (*27*), whereas BMP5 mutants lack external ears (*28*). Also, BMP4 and BMP7, regulated by the AER, were suggested to be involved in apoptosis of interdigital tissue (*29*). It is therefore possible that IKKα may somehow regulate the localized expression of certain BMPs.

References and Notes

1. P. A. Baeuerle, and D. Baltimore, *Cell* **87**, 13 (1996); I. M. Verma, J. K. Stevenson, E. M. Schwarz, D. Van Antwerp, S. Miyamoto, *Genes Dev.* **9**, 2723 (1995); A. A. Beg and A. S. Baldwin Jr., *ibid.* **7**, 2064 (1993).
2. J. A. DiDonato, M. Hayakawa, D. M. Rothwarf, E. Zandi, M. Karin, *Nature* **388**, 548 (1997); F. Mercurio *et al.*, *Science* **278**, 860 (1997); E. Zandi, D. M. Rothwarf, M. Delhase, M. Hayakawa, M. Karin, *Cell* **91**, 243 (1997).
3. C. H. Régnier *et al.*, *Cell* **91**, 373 (1997); J. D. Woronicz, X. Gao, Z. Cao, M. Rothe, D. V. Goeddel, *Science* **278**, 866 (1997).
4. E. Zandi, Y. Chen, M. Karin, *Science* **281**, 1360 (1998).
5. D. M. Rothwarf, E. Zandi, G. Natoli, M. Karin, *Nature* **395**, 297 (1998).
6. S. Yamaoka *et al.*, *Cell* **93**, 1231 (1998).
7. M. Delhase, M. Hayakawa, Y. Chen, M. Karin, *Science* **284**, 309 (1999).
8. An *Ikkα* clone was isolated from a 129/SV mouse genomic library (Stratagene). Bam HI fragments were subcloned in pUC18, mapped, and sequenced. A 1.5-kb Bam HI–Sac I fragment containing three exons encoding part of the kinase domain (amino acids 130 to 191) was cloned into the Xba I site of pGNA [H. LeMouellic, Y. Lallemand, P. Brulet, *Proc. Natl. Acad. Sci. U.S.A.* **87**, 4712 (1990)], and its 3′ end was fused in frame to the *LacZ* gene. A diphtheria toxin (DT-A) gene was inserted into the Kpn I site of the vector, and a 4-kb Nco I–Bam HI fragment containing a portion of the third exon (amino acids 213 to 232) and a large intron was cloned into the Apa I site. Homologous recombination between the linearized targeting vector and *Ikkα* should result in disruption of the *Ikkα* coding region and deletion of DNA encoding amino acids 192 to 212 of the kinase domain in supplementary Web Fig. 1 (*18*).
9. Figures 4 and 5 in supplementary Web material (*18*).
10. The targeting vector was linearized with Pme I and electroporated into R1 ES cells [A. Nagy, J. Rossant, R. Nagy, W. Abramow-Newerly, J. C. Roder, *Proc. Natl. Acad. Sci. U.S.A.* **90**, 8424 (1993)]. G418-resistant clones were expanded and analyzed by Southern (DNA) blotting for the presence of a disrupted *Ikkα* allele.
11. Three *Ikkα*$^{+/-}$ euploid ES cell clones were injected into C57Bl/6J blastocysts to derive chimeric mice [A. L. Joyner, Ed., *Gene Targeting: a Practical Approach* (IRL Press at Oxford Univ. Press, New York, 1993)]. Males with high degree of chimerism were crossed with C57Bl/6JxDBA females to generate *Ikkα*$^{+/-}$ mice.
12. Whole-cell extracts were prepared from muscles of E18 fetuses, and 200-μg samples were separated by SDS–polyacrylamide gel electrophoresis (PAGE), transferred to Immobilon membranes (Millipore), and probed with antibodies to IKKα, IKKβ, IKKγ, IκBα, IκBβ, IκBε, p65/RelA, and p52/NFκB2, as described (*5*).
13. P. Zhang and Y. Hu, unpublished results in supplementary Web Fig. 3 (*18*).
14. K. Benirschke and P. Kaufmann, *Pathology of the Human Placenta* (Springer-Verlag, New York, ed. 3, 1995).
15. G. Karsenty, *Dev. Genet.* **22**, 301 (1998); D. M. Kochhar, in *Handbook of Teratology*, J. G. Wilson and E. C. Fraser, Eds. (Plenum, New York and London, 1977), vol. 2, pp. 453–473; C. Tickle and G. Eichele, *Annu. Rev. Cell Biol.* **10**, 121 (1994).
16. Paraffin sections of normal and mutant embryos were dewaxed in xylene and rehydrated sequentially in 100, 95, 90, 70, and 0% ethanol in H_2O. Sections were then treated with proteinase K (20 μg/ml) at 37°C for 20 min and after washing with phosphate-buffered saline (PBS) were stained with In situ Cell Death Detection Kit (Boehringer Mannheim).
17. Pregnant mothers were injected intraperitoneally with BrdU (200 μg/g; Sigma) and killed after 2 hours. Fetuses (E17) were removed, fixed in 4% paraformaldehyde, and sectioned. Paraffin sections were stained with anti-BrdU and visualized by fluorescent immunohistochemistry with Tyramide Signal Amplification Kit (NEN/Life Science).
18. Supplementary Web material is available at www.sciencemag.org/feature/data/987144.shl.
19. M. Delhase, unpublished results. Although the extent of induction of NF-κB DNA binding activity was similar in WT and mutant fibroblasts, the total level of NF-κB binding activity was reproducibly lower (by a factor of 2) in the latter.
20. V. Baud and Y. Hu, unpublished results.
21. Q. Li, D. Van Antwerp F. Mercurio, K.-F. Lee, I. M. Verma, *Science* **284**, 321 (1999).
22. D. Morisato and K. V. Anderson, *Cell* **76**, 677 (1994); M. Meister, B. Lemaitre, J. A. Hoffmann, *BioEssays* **19**, 1019 (1997); M. Reach *et al.*, *Dev. Biol.* **180,** 353 (1996).
23. L. Burkly *et al.*, *Nature* **373**, 531 (1995); F. Kontgen *et al.*, *Genes Dev.* **9**, 1965 (1995); F. Weih *et al.*, *Cell* **80**, 331 (1995); W. C. Sha, H. C. Liou, E. I. Tuomanen, D. Baltimore, *ibid.*, p. 321.
24. Y. Kanegae, A. T. Tavares, J. C. I. Belmonte, I. M. Verma, *Nature* **392**, 611 (1998); P. B. Bushdid *et al.* *ibid.*, p. 615.
25. Z.-G. Liu, H. Hu, D. V. Goeddel, M. Karin, *Cell* **87**, 565 (1996); A. A. Beg and D. Baltimore, *Science* **274**, 782 (1996); D. J. Van Antwerp, S. J. Martin, T. Kafri, D. R. Green, I. M. Verma, *ibid.*, p. 787; C.-Y. Wang, M. W. Mayo, A. S. Baldwin Jr., *ibid.*, p. 784.
26. C. S. Seitz, Q. Lin, H. Deng, P. A. Khavari, *Proc. Natl. Acad. Sci. U.S.A.* **95,** 2307 (1998).
27. M. J. Solloway *et al.*, *Dev. Genet.* **22**, 321 (1998).
28. D. M. Kingsley *et al.*, *Cell* **71**, 399 (1992).
29. T. Katagiri, S. Boorla, J.-L. Frendo, B. L.M. Hogan, G. Karsenty, *Dev. Genet.* **22**, 340 (1998); B. Hogan, *Genes Dev.* **10**, 1580 (1996); D. M. Kingsley, *Trends Genet.* **10**, 16 (1994).

30. We thank G. Martin for critical comments; N. Varki, A. Ornoi, and K. Benirschke for helpful discussion and assistance with pathological and histological analyses; I. Verma for communication of unpublished results; and B. Thompson for manuscript preparation. Supported by grants from the National Institutes of Health (R37 ES04151 and R01 AI43477). Electron microscopy was supported by NIH grant RR04050. Y.H., V.B., and M.D. were supported by postdoctoral fellowships from the Arthritis Foundation San Diego Chapter, Human Frontier Science Project, and the D. Collen Research Foundation vzw. M.K. is a Frank and Else Schilling–American Cancer Society Research Professor.

16 December 1998; accepted 12 March 1999